Adaptive Meshes in Graph Neural Networks for Predicting Sea Surface Temperature through Remote Sensing

José G. Reyes[1][0009−0000−4700−1981], Giovanny A. C-Londoño[2][0000−0002−8368−7324] and Javier Sánchez[1][0000−0001−8514−4350]✉

[1] IU Cibernética, Empresas y Sociedad (IUCES)
[2] IU Investigación en Acuicultura Sostenible y Ecosistemas Marinos (ECOAQUA)
University of Las Palmas de Gran Canaria, Spain
{jose.reyes121,giovanny.cuervo101}@alu.ulpgc.es, jsanchez@ulpgc.es

Abstract. Accurate sea surface temperature (SST) forecasting is key for understanding marine and climatic dynamics, but remains challenging in high-variability regions such as coastal zones. Deep learning techniques have recently surpassed traditional numerical methods in computational efficiency and accuracy in prediction tasks. In particular, graph neural networks (GNNs) have demonstrated outstanding performance in forecasting climate variables and are attracting interest for modeling ocean dynamics. This work aims to adapt a GNN, originally designed for atmospheric data, to predict the temperature at the ocean surface. However, this type of neural network typically relies on regular meshes, which struggle to capture nonlinear oceanographic processes. Therefore, we propose to use a physically-informed mesh that adapts node density based on the bathymetry of the sea, prioritizing coastal areas. Our method integrates satellite-derived SST data with flexible graph topologies by restructuring latent representations through physics-aware graphs. The model is optimized with the L4 SST satellite images dataset from the Copernicus Marine Service. The results demonstrate that adaptive meshes reduce forecasting errors compared to regular grids, particularly near the coast. This approach bridges geospatial data and graph-based learning, showing that node allocation based on static forcings enhances model performance. The results highlight the potential of geometric deep learning for operational oceanography, offering improved interpretability and accuracy in complex geophysical systems based on remote sensing.

Keywords: Graph Neural Networks · Adaptive Mesh · Deep Learning · Sea Surface Temperature · Remote Sensing.

1 Introduction

Forecasting SST is a fundamental task in physical oceanography, with broad applications ranging from climate modeling and marine ecosystem management

to fisheries and extreme event prediction. Accurate SST predictions are especially significant in coastal regions, where dynamic processes such as upwelling, eddies, and thermal fronts exhibit complex and nonlinear behavior. While physically grounded, traditional numerical models often face limitations in computational cost and spatial resolution, particularly in high-variability areas where fine-grained predictions are needed.

In recent years, deep learning approaches, and specifically Graph Neural Networks (GNNs), have emerged as a promising alternative, offering flexible data representations and powerful capabilities to learn spatiotemporal patterns from remote sensing data [17, 9].

GNNs have demonstrated remarkable progress in various geophysical forecasting tasks, including weather prediction, traffic flow estimation, and now increasingly in oceanography. These models operate on graph-structured data, enabling them to model irregular domains and capture long-range spatial dependencies more effectively than traditional convolutional architectures. Recent works such as GraphCast [8], SeaCast [6], and GNN-Surrogate [16] have shown that GNNs can outperform conventional models, especially when deployed on large-scale Earth system datasets. However, a common limitation of most existing GNN-based prediction models is their reliance on fixed, uniform spatial discretizations, which fail to capture the spatial heterogeneity of ocean processes, particularly near the coast [15].

Recent advancements in adaptive graph techniques have addressed these shortcomings: i) Adaptive Graph Learning: Models like AGLNM [17] dynamically update the adjacency matrix during training via a graph loss mechanism, uncovering hidden spatial dependencies to improve SST prediction accuracy. SD-LPGC [9] further constructs static and dynamic graphs to capture long- and short-term spatial patterns with personalized convolutional filters; ii) Hierarchical and Multiscale Mesh Adaptation: To balance resolution and computational cost, GNN-Surrogate [16, 10] employs unstructured hierarchical meshes with adaptive resolutions, enabling efficient exploration of ocean simulation parameter spaces. Multiscale GNN architectures with Adaptive Mesh Refinement (AMR) [14] mimic multigrid solvers, locally refining nodes in regions that require high fidelity. iii) Attention Mechanisms and Memory Networks: GM-SAN [15] uses multi-head self-attention to extract global dependencies and build adaptive graphs among multiple SST points. Graph Memory Neural Networks (GMNN) [10] integrate a graph encoder with temporal LSTM modules to handle irregular SST regions and missing-data zones caused by islands or coastlines.

Graph Convolution Networks (GCN) coupled with Computational Fluid Dynamics (CFD) have demonstrated the ability to predict previously unseen flow behaviors [4], and tools like MeshCNN [5] and PolyGen [12] have advanced direct mesh analysis and generation with high accuracy and efficiency.

Anisotropic remeshing techniques [11] refine meshes based on geometric complexity and velocity gradients, concentrating resolution where needed. Moreover, studies reveal an inverse relationship between node count in Graph Element Net-

works (GENs) [1] and RMSE, with strategic node placement in high-complexity regions offering superior accuracy under limited computational budgets.

This paper addresses these issues by introducing a novel, physically-informed, mesh strategy for GNN-based SST forecasting. Instead of relying on uniformly distributed nodes, we propose a graph construction paradigm that adapts the spatial resolution based on the bathymetry. Our approach increases node density in coastal regions, where SST dynamics are more complex, and reduces it in deep ocean areas with more stable thermal patterns. This leads to the development of adaptive meshes that enhance the representational power of GNNs without incurring additional computational costs.

Our contributions are threefold: i) we propose a new mesh construction method where node density is inversely related to ocean depth, guided by bathymetric data, ensuring more accurate representation of SST dynamics in coastal zones; ii) we embed these adaptive meshes within a bipartite graph neural network inspired by GraphCast and SeaCast, incorporating a multi-resolution structure for efficient spatial information propagation; iii) we conduct experiments on the Canary current coastal upwelling system using the L4 SST dataset from the Copernicus Marine Service. Results show that our bathymetry-based mesh improves the performance of uniform mesh baselines, particularly in some regions near the coast.

The paper is organized as follows: Section 2 introduces the dataset and the architecture of our graph neural network, including the design of the proposed adaptive meshes. Section 3 presents the experimental results, evaluating the impact of different mesh strategies. Finally, Section 4 discusses implications, limitations, and directions for future research.

2 Methods and Data

To address the inherent limitations of regular grids in predicting dynamic coastal phenomena, we developed a novel methodology centered on adapting the underlying graph topology guided by relevant physical forcings. Our starting point is an initial graph with a regular grid structure, upon which we apply two successive transformations designed to optimize spatial representativeness in those regions where ocean dynamics exhibit greater complexity.

2.1 High Resolution SST Dataset

We use the High Resolution Level 4 Reprocessed SST dataset provided by the Copernicus Marine Service [2]. Our analysis focuses on the region of the Canary Islands and the northwest African coast, which is included within the spatial extent of this product.

This dataset provides daily gap-free SST maps classified as a Level 4 product. The horizontal resolution of these maps is $0.05^\circ \times 0.05^\circ$, allowing for detailed analysis of temperature structures in our area of interest.

The temporal extent of this dataset spans from January 1, 1982, to December 31, 2023, providing us with an extensive time series for training and evaluating our forecasting models. The product represents a daily-mean SST field at 20 cm depth. The data used to generate this product comes from satellite observations of the European Space Agency Sea Surface Temperature Climate Change Initiative (ESA SST CCI) for the period 1982-2016 and from the Copernicus Climate Change Service (C3S) L3 product for the period 2017 to present. The processing level is 4, meaning it is a spatially complete analysis.

We selected the spatial extent from latitude 19.55° to 34.52° N and longitude −20.97° to −5.98° E, which includes the Canary Islands and the northwest African coast, the focus of our study. This area is a subset of the original product's full domain. This dataset is updated annually and is available in NetCDF-4 format. This high-resolution and reprocessed dataset from the Copernicus Marine Service provides a solid and reliable basis for investigating the forecasting of SST in our area of interest.

2.2 Architecture of the Graph Neural Network

Our graph neural network architecture draws inspiration from the groundbreaking GraphCast model [8], which achieved major advancements in machine learning-based weather forecasting. Building on GraphCast's conceptual framework, Neural-LAM [13] introduced a similar encode-process-decode structure, as shown in Fig. 1, but employed a distinct bipartite graph design. This approach was later adapted by SeaCast [6] for specialized oceanographic applications [3]. Our work builds on the bipartite graph structure proposed by Neural-LAM and SeaCast, adapting it to model the complex, non-linear dynamics of the ocean.

The model works in an autoregressive way, $\hat{\mathbf{x}}^{t+1} = f(\mathbf{x}^t, \mathbf{x}^{t-1})$, where a future SST state $\hat{\mathbf{x}}^{t+1}$ is estimated from two previous time instants $\mathbf{x}^t$ and $\mathbf{x}^{t-1}$, mapped from a latitude-longitude grid into a graph-based representation.

The bipartite graph is denoted as $\mathcal{G}$ ($\mathcal{V}^g$, $\mathcal{V}^m$, $\mathcal{E}^m$, $\mathcal{E}^{g2m}$, $\mathcal{E}^{m2g}$), comprising two distinct sets of nodes: Grid nodes ($\mathcal{V}^g$) that are arranged in a regular grid, directly corresponding to the spatial structure of the input SST data given in matrix format. They serve as the initial representation of data; Mesh nodes ($\mathcal{V}^m$) that are organized in a hierarchical multi-level graph with three levels of resolution (L_1, L_2, L_3). Each subsequent coarser level contains progressively fewer nodes and longer-range connections, allowing for the representation of multiscale oceanographic processes; see Fig. 2. The focus of our contribution lies in adapting this multi-level mesh component.

Edges within the mesh connect its nodes ($\mathcal{E}^m$), while edges $\mathcal{E}^{g2m}$ and $\mathcal{E}^{m2g}$ facilitate information exchange between the grid nodes and the mesh nodes.

The *encoder* transforms the input data from the grid into the mesh with information about the location of each node. The *processor* comprises several layers that facilitate efficient local and global information propagation through message-passing mechanisms. Subsequently, the *decoder* projects the processed features back to the spatial grid, predicting the future state as a residual update.

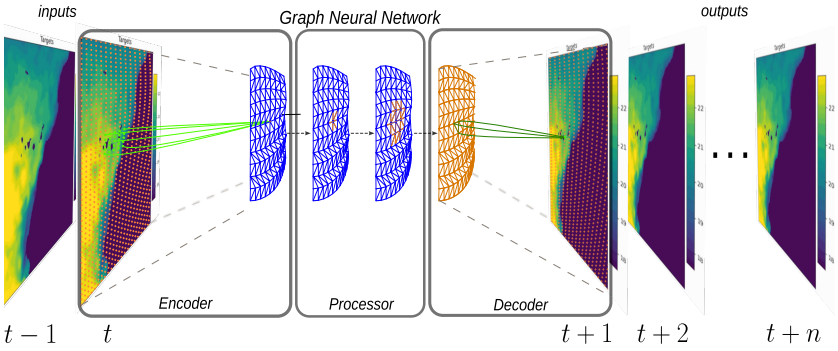

Fig. 1. The *encoder-processor-decoder* structure: The *encoder* embeds the information from the grid into the mesh; multiple message-passing steps are carried out in the layers of the *processor* to transform node features; the SST forecast is obtained at the *decoder*, which converts the mesh features into grid values. The grid, $\mathcal{V}^g$, is a regular map that contains the input SST data. The mesh, $\mathcal{V}^m$, processes the node features, sending information through the edges, $\mathcal{E}^m$. Grid pixels are sent to the mesh nodes through grid-to-mesh edges, $\mathcal{E}^{g2m}$, and back through mesh-to-grid edges, $\mathcal{E}^{m2g}$, represented in green lines.

The output of the decoder can then be fed into the system in an autoregressive way to forecast the SST over multiple days.

The training process is organized in two phases: In the first one, batches of three consecutive time instant samples are organized randomly, and the parameters of the network are calculated using the AdamW optimizer during 150 epochs; In the second phase, the samples are increased to contain up to four output estimates, so that the network can predict multiple forecasts in the future, optimizing the parameters for each lead time. The dataset is split into four years for the training set, one year for validation, and one year for the test set. Although the dataset covers 40 years, we selected 6 years due to the complexity of the neural network and our computational resources, which is enough to assess the model's performance.

One benefit of this model is that it can produce skillful medium-range forecasts significantly faster than traditional systems, achieving a full 10-day global forecast in under one minute on a single TPU device.

2.3 Mesh Configurations

In this work, we investigate the impact of various mesh configurations, $\mathcal{V}^m$, on the predictive performance of our GNN, particularly in the context of coastal upwelling. To overcome the limitations of the static grid configurations, particularly in capturing the complex dynamics of the coast, we developed a physically informed node densification mesh. We start with an initial regular grid and apply successive transformations to optimize spatial representativeness.

We compare the mesh configurations, each utilizing the same number of nodes at each corresponding level $\{L_1 : 3548,\ L_2 : 394,\ L_3 : 45\}$ for a fair comparison across our hierarchical graph structure. Table 1 shows the statistics of the three meshes.

Table 1. Mesh Statistics for each level (L_1, L_2, L_3) and configuration (Uniform, Random, Bathymetry-based), representing the number of nodes and edges, and the number of connections (min, max, avg) between nodes. At L_1, all three meshes have 3568 nodes, but the Uniform mesh has significantly more edges. The number of nodes decreases to 394 (L_2) and 45 (L_3), with the U-mesh maintaining approximately 20% and 10% more edges than the R-mesh and B-mesh at these levels and a higher average degree.

Mesh size	**Level 1**			**Level 2**			**Level 3**		
	U-mesh	R-mesh	B-mesh	U-mesh	R-mesh	B-mesh	U-mesh	R-mesh	B-mesh
Nodes	3568	3568	3568	394	394	394	45	45	45
Edges	27578	21216	21192	2848	2298	2248	268	242	208
Min degree	4	6	4	4	6	4	4	6	4
Max degree	16	24	26	16	22	22	16	16	20
Avg degree	15.46	11.89	11.88	14.46	11.66	11.41	11.91	10.76	9.24

Uniform Grided Mesh (U-mesh): Following the approach in [13, 6], this mesh is adapted to the geometry of the coastline, with nodes distributed regularly over the ocean domain and edges connecting the closest neighbors, forming potentially intersecting rectangular triangles (Fig. 2). This contrasts with more geometrically regular strategies employing non-intersecting equilateral triangles [7, 8].

Random Mesh (R-mesh): In this configuration, we place the nodes randomly in the mesh following a uniform distribution and create edges with Delaunay triangulation. The resulting graph has fewer edges than the U-mesh due to the absence of intersecting triangles, allowing us to assess the importance of regular node distribution and connection density.

Batimetry-based Mesh (B-mesh): This strategy distributes the nodes according to the bathymetry of the study area. Recognizing the higher SST variability in shallow waters, we concentrate more nodes in these areas and fewer in deeper and stable waters. Node placement follows the inverse probability of depth, $p(x) = \frac{1}{B(x)+\epsilon}$, with $B(x)$ being the bathymetry at point x and ϵ a small constant. The probability distribution function is given by $F(x) = \frac{p(x)}{\sum p(x)}$.

The hierarchical organization of all mesh configurations (U-mesh, R-mesh, and B-mesh) follows the structure proposed in [13], with connections between nodes at the same level (L_i) and across adjacent levels (L_{i-1} and L_{i+1}). Coarser levels (L_{i+1}) feature fewer nodes and long-range connections for efficient information propagation, while finer levels (L_{i-1}) have a higher node density and

shorter connections for modeling local interactions; see Fig. 2 and Table 1. Additionally, in our specific implementation of the bipartite graph, we have modified the connection strategy between $\mathcal{V}^g$ and $\mathcal{V}^m$ such that each $\mathcal{V}_i^g$ is consistently connected to exactly three nodes in $\mathcal{V}^m$ at level L_1. This differs from the original connection scheme in [13] and ensures a consistent information flow between the two graph components.

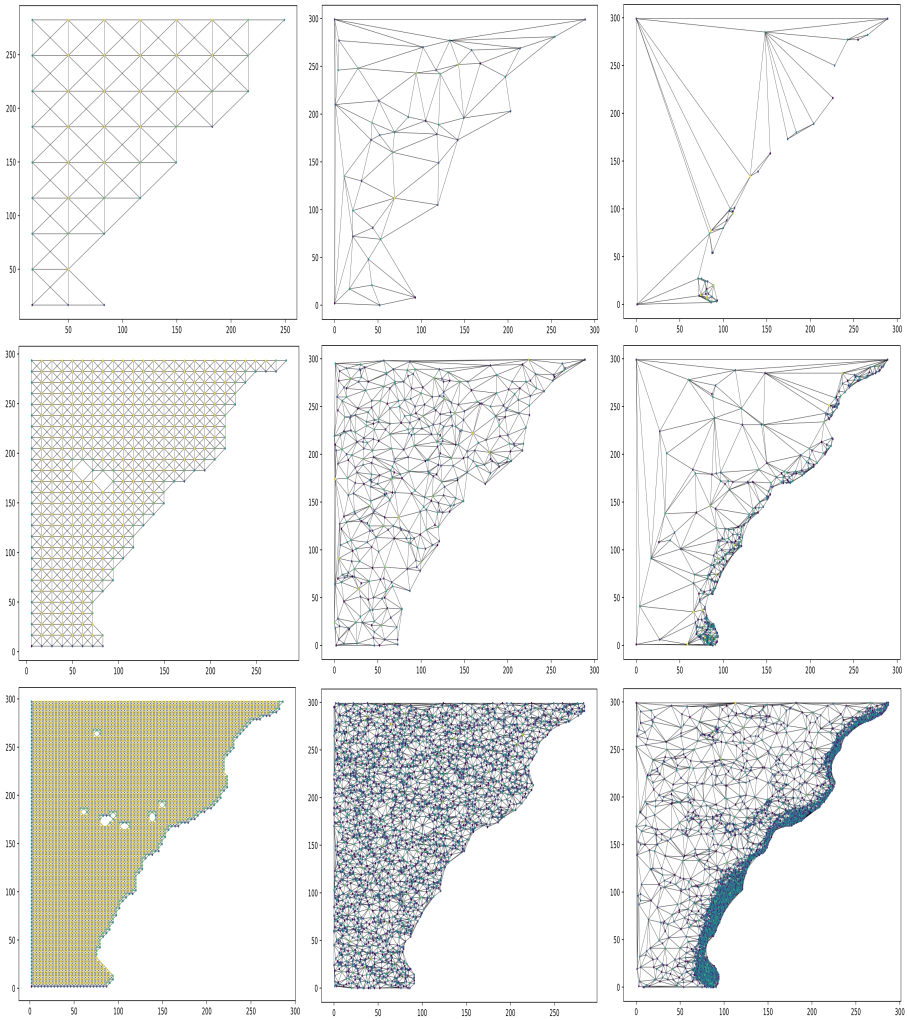

Fig. 2. Mesh configurations. The first column shows three levels of the uniform mesh (U-mesh); In the middle column, the random mesh (R-mesh); and the bathymetry-based mesh (B-mesh) on the right. The first row shows the coarsest scale, L_3, of each mesh, with fewer nodes and edges; the second row shows an intermediate scale, L_2; and the last row, the finest scale, L_1, with high density of nodes and edges.

These configurations will allow us to understand the influence of the distribution of nodes in the mesh and the number of edges between them. It will also allow us to study the accuracy improvement that results from the node density, especially in regions near the coast.

3 Results

In the experiments, the model was trained with the three mesh configurations, and we compared the RMSE score using the test dataset. A global assessment revealed that the random and bathymetry-based distributions did not yield a significant statistical reduction in RMSE over the entire domain. The mean RMSE remained virtually unchanged compared to the U-mesh baseline, indicating that the new meshes alone are insufficient to enhance overall accuracy. This is reasonable as the improvements are located in a small fraction of the domain.

However, the spatial analysis of the RMSE in Fig. 3 revealed a decrease in the upwelling area near the capes. In these locations, the RMSE improved by an average of 2.36% after applying the B-mesh. This localized improvement suggests that the concentration of nodes captures coastal processes more accurately.

Interestingly, when comparing the configurations separately by region, oceanic and coastal, with different total numbers of nodes each, we found that a sparse version, with approximately 75% fewer nodes in open waters, maintained the same level of accuracy without deteriorating the global performance. This suggests that the location of nodes is more relevant than their absolute quantity: removing nodes in areas with linear oceanic behavior does not penalize accuracy and reduces computational costs.

Although the RMSE was globally similar, the predictions made with the B-mesh showed greater spatial coherence and superior detail of mesoscalar filaments compared to the regular mesh, evidencing a more realistic resolution of upwelling structures (Fig. 4), with a moderate improvement near the capes.

These findings indicate that topological densification partially addresses the coast prediction problem; however, their global effectiveness requires a broader combination of forcings and optimization criteria to achieve consistent RMSE reductions across the entire ocean domain. The results reveal that the adaptive redistribution of nodes in geometric graphs applied to oceanographic prediction models offers limited improvements but provides valuable insights into the interaction between mesh topology, physical forcings, and local accuracy.

The localized reduction of RMSE in the capes was not only due to node density, but also to the coincidence between the adaptive mesh and a real physical pattern, underscoring that the alignment between graph topology and relevant forcings is crucial in areas where the forcing is the leading mechanism.

As anticipated in Section 2, densification based exclusively on bathymetry imposes a bias: it favors shallow areas without guaranteeing that these correspond to processes of interest. This bias was evident in regions where upwelling showed no direct correlation with depth, resulting in an inefficient redistribution of computational resources. Therefore, although a quality improvement of the

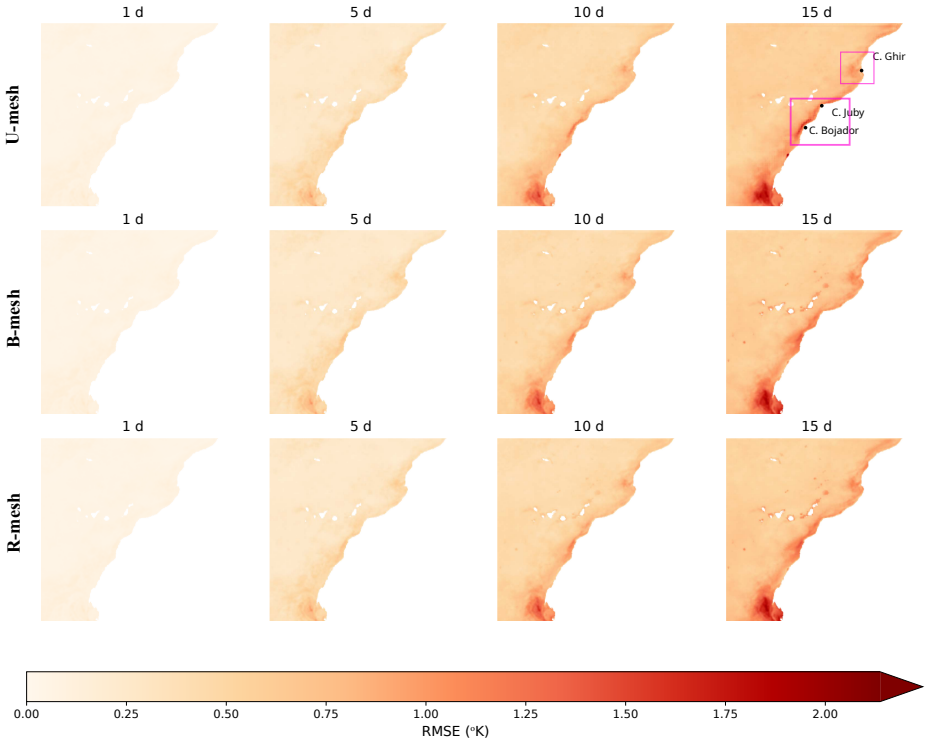

Fig. 3. Spatial RMSE maps in SST prediction for days 1, 5, 10, and 15, using the three mesh configurations. The U-mesh presents artifacts with square patterns, especially visible from day 10 onwards. In all cases, the error is mainly concentrated in coastal zones, especially near the capes. However, the B-mesh shows a qualitative improvement by reducing these localized errors and adapting better to the oceanic topography. Squares in the top-right map highlight regions where the differences are more significant (see Fig. 4 for a close-up).

predictions was achieved, there was no significant improvement in the model's accuracy.

One important finding was that reducing the number of nodes did not compromise accuracy in regions of low variability. In the open ocean, where conditions approach a quasi-linear regime, the decrease in nodes allowed for maintaining predictive performance while reducing computational cost. This result challenges the common assumption that increasing the density improves the accuracy. Instead, it suggests that an intelligent distribution, based on the underlying dynamics, is more effective than a dense mesh.

These findings align with previous research that demonstrates higher precisions by strategically positioning nodes in areas of high nonlinearity [1, 10]. However, our approach emphasizes that it is not enough to guide densification by bathymetry but also by its physical dynamics.

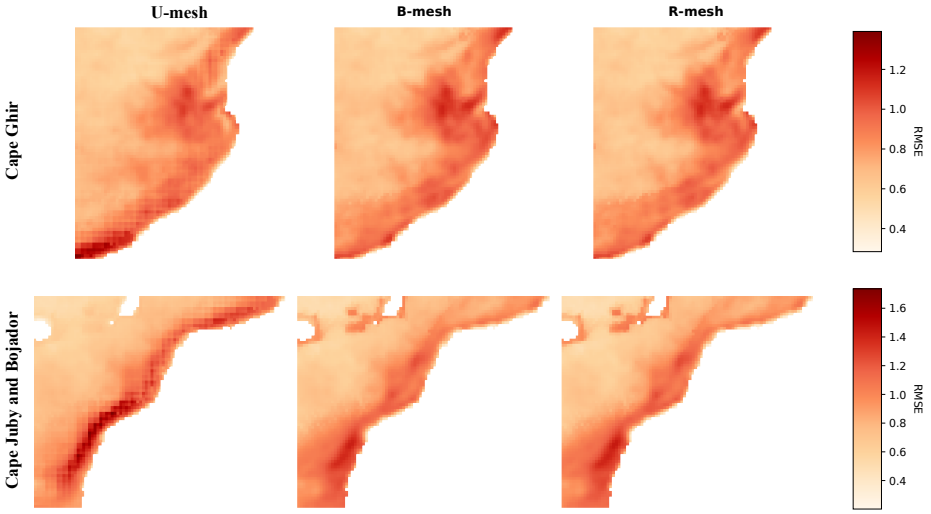

Fig. 4. RMSE in °K for the U-, B-, and R-mesh configurations across subdomains: Cape Ghir, Juby, and Bojador. The U-mesh exhibits square-shaped artifacts due to its grid configuration and higher RMSE near the coast. Some qualitative improvements are observed for the B- and R-meshes, especially in capes Juby and Bojador, as reflected in lower RMSE values. No artifacts are visible in these cases.

4 Conclusion

This work presented a novel approach to SST forecasting by integrating physically informed adaptive meshes into a GNN framework. By leveraging bathymetric information to redistribute mesh node density—particularly in high-variability coastal zones—the proposed method addresses limitations inherent in uniform grid models, which often struggle to capture nonlinear ocean dynamics.

Three mesh configurations were evaluated: a uniform grid (U-mesh), a random distribution (R-mesh), and a bathymetry-based adaptive mesh (B-mesh). While global forecasting performance, as measured by RMSE, remained largely unchanged, the B-mesh demonstrated clear improvements in coastal regions and capes. It attains similar results with far fewer edges, reducing computational complexity. These localized accuracy gains underscore the value of incorporating physical priors into graph topology design, enhancing model performance where fine-scale resolution is needed.

The study revealed that reasonable node placement can match or surpass dense uniform meshes while reducing computational overhead. This finding suggests that strategic mesh adaptation offers a more efficient and scalable path for geophysical forecasting models. Qualitatively, B-mesh forecasts exhibited greater spatial coherence and finer representation of mesoscale structures.

Future work will explore multi-modal physical forcings, such as ocean currents, wind patterns, and temperature gradients, as drivers for mesh refinement. Integrating domain knowledge with geometric deep learning holds significant potential for advancing operational oceanography and climate modeling from remote sensing.

Disclosure of Interests. The authors have no competing interests to declare that are relevant to the content of this article.

References

1. Alet, F., Jeewajee, A.K., Bauza, M., Rodriguez, A., Lozano-Perez, T., Pack Kaelbling, L.: Graph Element Networks: adaptive, structured computation and memory. arXiv e-prints arXiv:1904.09019 (Apr 2019). https://doi.org/10.48550/arXiv.1904.09019
2. CMEMS: European north west Shelf/Iberia Biscay Irish seas - high resolution L4 sea surface temperature reprocessed (2024), https://doi.org/10.48670/moi-00153
3. Cuervo-Londoño, G.A., Sánchez, J., Rodríguez-Santana, A.: Deep learning weather models for subregional ocean forecasting: A case study on the canary current upwelling system. Tech. rep. (2025), https://arxiv.org/abs/2505.24429
4. de Avila Belbute-Peres, F., Economon, T.D., Zico Kolter, J.: Combining Differentiable PDE Solvers and Graph Neural Networks for Fluid Flow Prediction. arXiv e-prints arXiv:2007.04439 (Jul 2020). https://doi.org/10.48550/arXiv.2007.04439
5. Hanocka, R., Hertz, A., Fish, N., Giryes, R., Fleishman, S., Cohen-Or, D.: MeshCNN: A Network with an Edge. arXiv e-prints arXiv:1809.05910 (Sep 2018). https://doi.org/10.48550/arXiv.1809.05910
6. Holmberg, D., Clementi, E., Roos, T.: Regional ocean forecasting with hierarchical graph neural networks. arXiv e-prints arXiv:2410.11807 (Oct 2024), http://doi.org/10.48550/arXiv.2410.11807
7. Keisler, R.: Forecasting global weather with graph neural networks. Tech. rep., Cornell University (2022), https://doi.org/10.48550/arXiv.2202.07575
8. Lam, R., Sánchez-González, A., Willson, M., Wirnsberger, P., Fortunato, M., Alet, F., Ravuri, S., Ewalds, T., Eaton-Rosen, Z., Hu, W., Merose, A., Hoyer, S., Holland, G., Vinyals, O., Stott, J., Pritzel, A., Mohamed, S., Battaglia, P.: Learning skillful medium-range global weather forecasting. Science **382**(6677), 1416–1421 (2023). https://doi.org/10.1126/science.adi2336
9. Li, X., Zhang, G., Huang, K., He, Z.: Towards spatio-temporal sea surface temperature forecasting via static and dynamic learnable personalized graph convolution network. Tech. rep., Cornell University (2023). https://doi.org/10.48550/arXiv.2304.09290
10. Lou, G., Zhang, J., Zhao, X., Zhou, X., Li, Q.: A non-uniform grid graph convolutional network for sea surface temperature prediction. Remote Sensing **16**(17) (2024). https://doi.org/10.3390/rs16173216
11. Narain, R., Samii, A., O'Brien, J.F.: Adaptive anisotropic remeshing for cloth simulation. ACM Transactions on Graphics **31**(6), 147:1–10 (Nov 2012). https://doi.org/10.1145/2366145.2366171, proceedings of ACM SIGGRAPH Asia 2012, Singapore

12. Nash, C., Ganin, Y., Eslami, S.M.A., Battaglia, P.W.: PolyGen: An Autoregressive Generative Model of 3D Meshes. arXiv e-prints arXiv:2002.10880 (Feb 2020). https://doi.org/10.48550/arXiv.2002.10880
13. Oskarsson, J., Landelius, T., Lindsten, F.: Graph-based neural weather prediction for limited area modeling. In: NeurIPS 2023 Workshop on Tackling Climate Change with Machine Learning (2023)
14. Perera, R., Agrawal, V.: Multiscale graph neural networks with adaptive mesh refinement for accelerating mesh-based simulations. Tech. rep., Cornell University (2024). https://doi.org/10.1016/j.cma.2024.117152
15. Sheng, L., Xu, L., Yu, J., and, Z.L.: A graph multi-head self-attention neural network for the multi-point long-term prediction of sea surface temperature. Remote Sensing Letters **14**(8), 786–796 (2023). https://doi.org/10.1080/2150704X.2023.2240506
16. Shi, N., Xu, J., Wurster, S.W., Guo, H., Woodring, J., Van Roekel, L.P., Shen, H.W.: GNN-Surrogate: A hierarchical and adaptive graph neural network for parameter space exploration of unstructured-mesh ocean simulations. IEEE Transactions on Visualization and Computer Graphics **28**(6), 2301–2313 (2022). https://doi.org/10.1109/TVCG.2022.3165345
17. Wang, T., Li, Z., Geng, X., Jin, B., Xu, L.: Time series prediction of sea surface temperature based on an adaptive graph learning neural model. Future Internet **14**(6) (2022). https://doi.org/10.3390/fi14060171